Editors' Suggestion

# Electron–$K$-phonon interaction in twisted bilayer graphene

Chao-Xing Liu,[1,2,*] Yulin Chen,[3] Ali Yazdani,[2] and B. Andrei Bernevig[2,4,5,*]
[1]*Department of Physics, The Pennsylvania State University, University Park, Pennsylvania 16802, USA*
[2]*Department of Physics, Princeton University, Princeton, New Jersey 08544, USA*
[3]*Department of Physics, University of Oxford, Oxford OX1 3PU, United Kingdom*
[4]*Donostia International Physics Center, P. Manuel de Lardizabal 4, 20018 Donostia-San Sebastian, Spain*
[5]*IKERBASQUE, Basque Foundation for Science, Plaza Euskadi 5, 48009, Bilbao, Spain*

(Received 24 March 2023; revised 1 May 2024; accepted 13 June 2024; published 17 July 2024)

We develop an analytic theory to describe the interaction between electrons and $K$ phonons and study its influence on superconductivity in the *bare bands* of twisted bilayer graphene (TBG). We find that, due to symmetry and the two-center approximation, only one optical $K$ phonon ($\sim$160 meV) of graphene is responsible for the intervalley electron-phonon interaction. This phonon has recently been found in angular-resolved photoemission spectroscopy to be responsible for replicas of the TBG flat bands. By projecting the interaction to the TBG flat bands, we perform the full symmetry analysis of the phonon-mediated attractive interaction and pairing channels in the Chern basis, and show that several channels are guaranteed to have gapless order parameters. From the linearized gap equations, we find that the highest $T_c$ pairing induced by this phonon is a singlet gapped $s$-wave inter-Chern-band order parameter, followed closely by a gapless nematic $d$-wave intra-Chern-band order parameter. We justify these results analytically, using the topological heavy-fermion mapping of TBG which has allowed us to obtain an analytic form of a phonon-mediated attractive interaction and to analytically solve the linearized and $T = 0$ gap equations. For the intra-Chern-band channel, the nematic state with nodes is shown to be stabilized in the chiral flat-band limit. While the flat-band Coulomb interaction can be screened sufficiently enough—around the Van Hove singularities—to allow for electron-phonon based superconductivity, it is unlikely that this effect can be maintained in the lower density of states excitation bands around the correlated insulator states.

DOI: 10.1103/PhysRevB.110.045133

## I. INTRODUCTION

Superconductivity in twisted bilayer graphene (TBG) appears within its phase diagram around the correlated insulator states [1–19]. Among the mechanisms suggested for superconductivity are phonons, spin fluctuations, skyrmions, and others [20–45]. Based on a recent experiment that suggests a strong coupling between the graphene $K$ phonon and the flat bands in TBG [46], we perform a comprehensive analysis of the electron–$K$-phonon (e-K-ph) interaction and the resulting phonon-mediated superconductivity on the bare flat bands of TBG. We develop an exhaustive numerical, analytical, and symmetry based description of the e-K-ph interaction in TBG and the symmetry classifications of the order parameter, and find the competing singlet gapped inter-Chern-band channel and nematic gapless intra-Chern-band channel. Armed with the heavy-fermion description of TBG [47–55], the form factors of the $K$-phonon induced attractive interaction can be analytically computed and matched well to full numerical calculations. An analysis of the Coulomb screening shows that, due to the high density of states (DOS) of flat bands, the Coulomb interaction might be strongly renormalized down near the Van Hove singularities. However, it remains unclear if the Hartree-Fock bands of the correlated insulator, with the lower DOS, can provide a similar result.

## II. MODEL HAMILTONIAN FOR ELECTRON-PHONON INTERACTION IN TBG

We consider the deformation potential type of theory, described by a tight-binding (TB) model for the electron Hamiltonian with the hopping parameters depending on the atom positions $\tilde{\mathbf{R}}^l_\alpha = \mathbf{R}^l + \tau^l_\alpha + \mathbf{u}^l(\mathbf{R}^l_\alpha)$ with a displacement field $\mathbf{u}^l(\mathbf{R}^l_\alpha = \mathbf{R}^l + \tau^l_\alpha)$, where $\mathbf{R}^l$ and $\tau^l_\alpha$ label the lattice vector and the sublattice atom position ($\alpha = A, B$) at the layer $l$, respectively. By treating $\mathbf{u}$ as a perturbation, we expand the intralayer Hamiltonian up to the linear order in $\mathbf{u}$ [Supplemental Material (SM) Sec. II [56]]. We only keep $\mathbf{u}$-independent terms for the interlayer Hamiltonian for TBG, thus focusing on the intralayer electron-phonon (e-ph) interaction in this paper. As only the Dirac bands appear around the Fermi energy close to $\pm\mathbf{K}_D = \pm\frac{4\pi}{3a_0}(1, 0)$ in the Brillouin zone (BZ) with the lattice constant $a_0$ in graphene, we also expand the Hamiltonian around $\eta\mathbf{K}_D$ ($\eta = \pm$ labeling two valleys) and focus on Dirac electrons around two valleys. Our full Hamiltonian consists of three parts,

$$H = H_{\rm el} + H_{\rm ph} + H_{\rm eph}. \tag{1}$$

Here, $H_{\rm el}$ describes the Dirac electrons located at valley $\eta = \pm$ momentum $\eta\mathbf{K}_D$ that are coupled through interlayer tunnelings and is given by the Bistritzer-MacDonald (BM) model

*These authors contributed equally to this work.

 

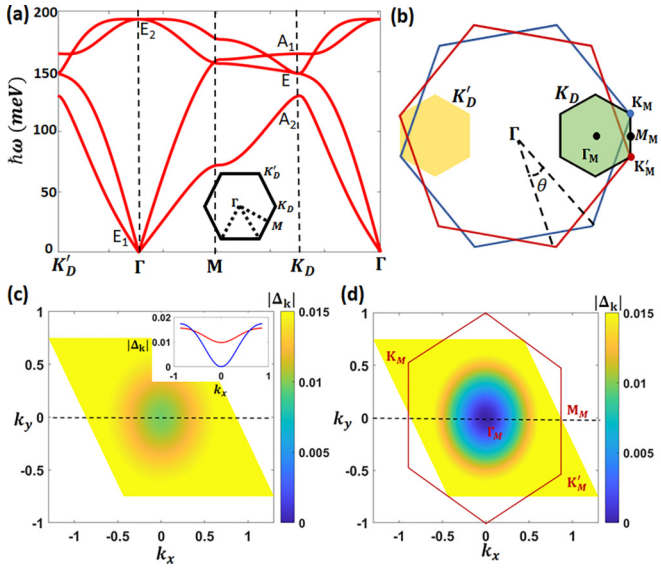


FIG. 1. (a) Phonon dispersion of graphene. The irreps for phonon modes at $\Gamma$ and $\mathbf{K}_D$ are labeled. Inset: BZ of graphene. (b) MBZ of TBG. (c) and (d) show the momentum dependence of the normalized gap function $|\Delta_{\mathbf{k}}|$ for the inter-Chern-band $A_1$ singlet (or the $A_2$ triplet) channel and intra-Chern-band pairing 2D $E_2$ singlet channel, respectively. The inset in (c) shows the $|\Delta_{\mathbf{k}}|$ along the dashed line $k_y = 0$ for both the inter-Chern-band (red) and intra-Chern-band (blue) channels. The momenta $\mathbf{\Gamma}_M$, $\mathbf{K}_M$, $\mathbf{M}_M$ are labeled in MBZ in (b) and (d).

[57] (SM Sec. V [56]),

$$\hat{H}_{\rm el} = \sum_{\eta s} \sum_{\mathbf{k}\in\mathrm{MBZ}} \sum_{\alpha\alpha'} \sum_{\mathbf{Q},\mathbf{Q}'} h^{(\eta)}_{\mathbf{Q}\alpha,\mathbf{Q}'\alpha'}(\mathbf{k}) c^{\dagger}_{\mathbf{k},\mathbf{Q},\alpha,\eta,s} c_{\mathbf{k},\mathbf{Q}',\alpha',\eta,s}, \quad (2)$$

where $c_{\mathbf{k},\mathbf{Q},\alpha,\eta,s}$ is the fermion annihilation operator, $\mathbf{k}$ is a momentum in the moiré Brillouin zone (MBZ) [Fig. 1(b)], $\alpha$ is the sublattice index, and $s$ is spin. The vector $\mathbf{Q}$ belongs to the lattice set $\mathcal{Q}_{l\eta} = \{l\eta\mathbf{q}_2 + n_1\mathbf{b}_{M1} + n_2\mathbf{b}_{M2} \,|\, n_{1,2} \in \mathbb{Z}\}$, where $l$ is the layer index, $\mathbf{q}_2 = k_\theta(\frac{\sqrt{3}}{2}, \frac{1}{2})$, $\mathbf{b}_{M1} = k_\theta(\frac{\sqrt{3}}{2}, \frac{3}{2})$, $\mathbf{b}_{M2} = k_\theta(-\frac{\sqrt{3}}{2}, \frac{3}{2})$, and $k_\theta = 2|\mathbf{K}_D| \sin\frac{\theta}{2}$ with $\theta$ the twist angle. $h^{(\eta)}_{\mathbf{Q}\alpha,\mathbf{Q}'\alpha'}(\mathbf{k})$ is given in SM Sec. V A [56]. $\hat{H}_{\rm el}$ exhibits $C_{6v}$ and time-reversal symmetries, generated by valley-switching $\pi/6$ rotation along the $z$ axis ($\hat{C}_{6z}$), time reversal ($\hat{T}$), and $\pi$ rotation along the $y$ axis ($C_{2y}$), and valley-preserving $\pi$ rotation along the $x$ axis ($\hat{C}_{2x}$), and the composite antiunitary $C_{2z}T$. In addition, $\hat{H}_{\rm el}$ has a unitary particle-hole ($\hat{P}$) symmetry, as well as a chiral symmetry $\hat{C}$ in the limit with vanishing $AA$ region hopping ($w_0 = 0$) [19]. A full discussion of symmetry of the BM model [58,59] is found in SM Sec.V B [56] (see also Refs. [60–63] therein).

$H_{\rm ph}$ describes the intralayer in-plane phonon modes. Out-of-plane phonon modes are decoupled from Dirac electrons for the intralayer e-ph interaction. The dynamical matrix for a single-layer graphene is derived in SM Sec. III [56] based both on symmetry considerations and the microscopic model, up to the next-nearest-neighbor interaction. The resulting in-plane phonon dispersion in Fig. 1(a) reproduces that in the literature [64–68] (SM Secs. III and IV B [56]). The phonon modes at $\Gamma$ and $\eta\mathbf{K}_D$ can induce intravalley and intervalley e-ph interactions, respectively. In this paper we focus on the $\eta\mathbf{K}_D$ phonons. At $\eta\mathbf{K}_D$, we have one $A_1$ ($\sim$160 meV), one $A_2$ ($\sim$140 meV), and one two-dimensional (2D) $E$ mode ($\sim$150 meV) of the $C_{3v}$ group. Based on the deformation potential theory, we derive the e-ph interaction $H_{\rm eph}$ by expanding the TB Hamiltonian treating both the momentum and phonon displacement field $\mathbf{u}$ as perturbations. For the e-ph interaction, we only keep the dominant zeroth order in momentum for the $\eta\mathbf{K}_D$ phonons. We find, due to both symmetry and the two-center approximation (SM Sec. II E [56]), that only the $A_1$ phonons at $\mathbf{K}_D$ can scatter an electron from $\mathbf{K}_D$ to $-\mathbf{K}_D$ [68]. The corresponding Hamiltonian reads

$$H^{\mathrm{op},A_1}_{\mathrm{intervall}} \approx \frac{\gamma_3}{\sqrt{2N_G M\omega_{A1}}} \sum_{\tilde{\mathbf{k}},\tilde{\mathbf{k}}',\eta,\alpha\beta} (b_{-\eta\mathbf{K}_D+\tilde{\mathbf{k}}-\tilde{\mathbf{k}}',A_1} + b^{\dagger}_{\eta\mathbf{K}_D-\tilde{\mathbf{k}}+\tilde{\mathbf{k}}',A_1}) c^{\dagger}_{\tilde{\mathbf{k}}+\eta\mathbf{K}_D,\alpha} (\sigma_x)_{\alpha\beta} c_{\tilde{\mathbf{k}}'-\eta\mathbf{K}_D,\beta}, \quad (3)$$

where $\tilde{\mathbf{k}}$ is the electron momentum away from $\eta\mathbf{K}_D$, $N_G$ is the number of atomic unit cells, $M$ is the atomic mass, $\omega_{A1}$ is the $A_1$ phonon frequency, and $b$ and $c$ are phonon and electron annihilation operators. The material-dependent parameter $\gamma_3$ can be derived from the hopping potential as $\gamma_3 = 2i\sum_{\mathbf{G}} e^{i(\tau_A-\tau_B)\cdot\mathbf{G}}(\mathbf{G}+\mathbf{K}_D)_y t(\mathbf{G}+\mathbf{K}_D, 0) \approx 17$ eV/ Å, where $\mathbf{G}$ is the reciprocal lattice vector and $t(\mathbf{q})$ is the Fourier transform of the $\pi$-bond hopping function between two carbon $p_z$ orbitals in graphene [Eq. (6) in SM Sec. I [56]]. Our next step is to rewrite the electron momentum $\tilde{k}$ into the MBZ by $\tilde{\mathbf{k}} = \mathbf{k} - \mathbf{Q}_{l\eta}$ with $\mathbf{k} \in$ MBZ, so that $c_{\mathbf{k},\mathbf{Q}_{l\eta},\alpha,\eta,s} = c_{\eta\mathbf{K}^l_D+\tilde{\mathbf{k}},\alpha,l,s}$ and $\sum_{\tilde{\mathbf{k}}} \to \sum_{\mathbf{k}\in\mathrm{MBZ}}\sum_{\mathbf{Q}_{l\eta}}$, where we have added the spin index $s$ and layer index $l$. Finally, we project the e-ph interaction $H^{\mathrm{op},A_1}_{\mathrm{intervall}}$ into the flat bands of the BM Hamiltonian as

$$H^{\mathrm{op},A_1}_{\mathrm{intervall}} \approx \frac{1}{\sqrt{N_G}} \sum G^{\eta nn'l}_{\mathbf{k},\mathbf{k}',\mathbf{Q}_{-l\eta}} \gamma^{\dagger}_{\mathbf{k},n,\eta,s} \gamma_{\mathbf{k}',n',-\eta,s} \times (b_{-\eta\mathbf{K}_D+\mathbf{k}-\mathbf{k}'-\mathbf{Q}_{-l\eta},l,A_1} + b^{\dagger}_{\eta\mathbf{K}_D-\mathbf{k}+\mathbf{k}'+\mathbf{Q}_{-l\eta},l,A_1}), \quad (4)$$

where the summation includes $\mathbf{k}$, $\mathbf{k}'$, $n$, $n'$, $\eta$, $s$, $l$, $\mathbf{Q}_{-l\eta}$, $\gamma^{\dagger}_{\mathbf{k},n,\eta,s} = \sum_{\mathbf{Q}\alpha} u_{\mathbf{Q}\alpha;n\eta}(\mathbf{k}) c^{\dagger}_{\mathbf{k},\mathbf{Q},\eta,\alpha s}$ with $u^n_{\mathbf{k},\mathbf{Q}'_{l\eta},\alpha,\eta}$ the eigenstates of $h^{(\eta)}_{\mathbf{Q}\alpha,\mathbf{Q}'\alpha'}(\mathbf{k})$. The matrix element

$$G^{\eta nn'l}_{\mathbf{k},\mathbf{k}',\mathbf{Q}_{-l\eta}} = \frac{\gamma_3}{\sqrt{2M\omega_{A_1}}} \sum_{\mathbf{Q}'_{l\eta},\alpha\beta} \times u^{n\star}_{\mathbf{k},\mathbf{Q}'_{l\eta},\alpha,\eta} \sigma^x_{\alpha\beta} u^{n'}_{\mathbf{k}',\mathbf{Q}'_{l\eta}-\mathbf{Q}_{-l\eta},\beta,-\eta} \quad (5)$$

characterizes the e-ph interaction strength for TBG and can be evaluated numerically (and later analytically), as shown in SM Sec. VI F [56]. We focus on two flat bands (per valley per spin) of TBG, labeled by $n = \pm$. Instead of the eigenstate basis, we work on the so-called "Chern-band" basis, defined by

$$u^{e_Y}_{\mathbf{k},\mathbf{Q},\alpha,\eta} = \frac{1}{\sqrt{2}}(u^{n=+}_{\mathbf{k},\mathbf{Q},\alpha,\eta} + ie_Y u^{n=-}_{\mathbf{k},\mathbf{Q},\alpha,\eta}), \quad (6)$$

with $e_Y = \pm 1$. $u^{e_Y}_{\mathbf{k},\mathbf{Q},\alpha,\eta}$ carries the Chern number $\pm 1$. On the Chern-band basis, the expressions for the e-ph interaction can be obtained by replacing the $n, n'$ indices in Eqs. (4) and

(5) with $e_Y, e'_Y$ indices and $u^{n}_{\mathbf{k},\mathbf{Q},\alpha,\eta}$ in Eq. (5) with $u^{e_Y}_{\mathbf{k},\mathbf{Q},\alpha,\eta}$. Discrete symmetries can constrain the form of the function $G^{\eta e_Y e'_Y l}_{\mathbf{k},\mathbf{k}',\mathbf{Q}_{-l\eta}}$, as discussed in SM Sec.VI D [56]. In particular, in the chiral limit $w_0 = 0$ one can show that $G^{\eta e_Y e'_Y l}_{\mathbf{k},\mathbf{k}',\mathbf{Q}_{-l\eta}} = \delta_{e_Y,e'_Y} G^{\eta e_Y e_Y l}_{\mathbf{k},\mathbf{k}',\mathbf{Q}_{-l\eta}}$ has a diagonal form on the Chern-band basis, and this approximation will be adopted below for the discussion of possible superconducting channels.

## III. PHONON-MEDIATED ELECTRON-ELECTRON INTERACTION AND SYMMETRY CLASSIFICATION OF SUPERCONDUCTING PAIRING CHANNELS

We next apply the Schrieffer-Wolff transformation [69] to integrate out the phonon modes and obtain the phonon-mediated electron-electron (el-el) interaction [25,32]. We focus on the Cooper pair channel of the attractive interaction, which takes the form

$$H_{ee} = -\frac{1}{N_M} \sum_{\mathbf{k},\mathbf{k}',s,s_1,e_Y,e'_Y} V^{\eta,e_Y,e'_Y}_{\mathbf{k},\mathbf{k}'} \times \gamma^{\dagger}_{\mathbf{k}e_Y\eta s} \gamma^{\dagger}_{-\mathbf{k}e'_Y,-\eta s_1} \gamma_{-\mathbf{k}'e'_Y,\eta s_1} \gamma_{\mathbf{k}'e_Y,-\eta s}, \tag{7}$$

where

$$V^{\eta,e_Y,e'_Y}_{\mathbf{k},\mathbf{k}'} = \frac{1}{N_0\omega_{A_1}} \sum_{\mathbf{G}_M,l} G^{\eta,e_Y,l}_{\mathbf{k},\mathbf{k}',-l\eta\mathbf{q}_2+\mathbf{G}_M} G^{-\eta,e'_Y,l}_{-\mathbf{k},-\mathbf{k}',l\eta\mathbf{q}_2-\mathbf{G}_M},$$

with $\mathbf{G}_M$ the moiré reciprocal lattice vectors, $N_M$ the number of moiré unit cells, and $N_0$ the number of atomic unit cells in one moiré unit cell ($N_G = N_0 \times N_M$). Discrete symmetries constrain the form of the interaction parameter $V^{\eta,e_Y,e'_Y}_{\mathbf{k},\mathbf{k}'}$. The ones leaving the momentum $(\mathbf{k},\mathbf{k}')$ unchanged are as follows: (1) $\hat{C}_{2z}\hat{P}$: $V^{\eta,e_Y,e'_Y}_{\mathbf{k},\mathbf{k}'} = V^{-\eta,e_Y,e'_Y}_{\mathbf{k},\mathbf{k}'}$; (2) $\hat{C}_{2z}\hat{T}$: $V^{\eta,e_Y,e'_Y}_{\mathbf{k},\mathbf{k}'} = V^{\eta,-e_Y,-e'_Y\star}_{\mathbf{k},\mathbf{k}'}$; and (3) the combination of index reshuffling and $\hat{P}$ symmetry: $V^{\eta,e_Y e'_Y}_{\mathbf{k},\mathbf{k}'} = V^{-\eta,e'_Y e_Y}_{\mathbf{k},\mathbf{k}'}$. These three symmetry operations reduce the number of the independent components of the $V$ function for a fixed $(\mathbf{k},\mathbf{k}')$ from eight complex parameters to one real ($V^{+,+-}_{\mathbf{k},\mathbf{k}'}$) and one complex parameter ($V^{+,++}_{\mathbf{k},\mathbf{k}'}$). Other discrete symmetries, including $\hat{P}$, reshuffling, Hermiticity, $\hat{C}_{3z}$, and $\hat{C}_{2z}$, relate the $V$ function at different $(\mathbf{k},\mathbf{k}')$. In particular, $\hat{C}_{3z}$ guarantees $V^{\eta,e_Y,e_Y}_{\mathbf{K}_M,0} = 0$ for the intra-Chern-band channels. The projected Coulomb interaction into the flat bands of the BM model possesses a large $U(4) \times U(4)$ spin-valley continuous symmetry [18,58,70]. The el-el interaction (7) breaks this symmetry down to the $U(2)_{e_Y=+} \times U(2)_{e_Y=-}$ in the chiral limit and further to a total spin $SU(2)$ together with a valley charge $U(1) \otimes U(1)$ (SM Sec. VI E [56]).

At the mean-field level, the attractive interaction (7) is decomposed into the fermion bilinear form $H_\Delta = \hat{\Delta} + \hat{\Delta}^\dagger$ with

$$\hat{\Delta} = \sum \gamma^{\dagger}_{\mathbf{k},e_{Y_1},\eta,s_1} \Delta^{\eta}_{\mathbf{k};e_{Y_1}s_1,e_{Y_2}s_2} \gamma^{\dagger}_{-\mathbf{k},e_{Y_2},-\eta,s_2}, \tag{8}$$

where the summation above includes the indices $\mathbf{k}$, $e_{Y_1}$, $e_{Y_2}$, $s_1$, $s_2$, $\eta$, and the gap function

$$\Delta^{\eta}_{\mathbf{k};e_{Y_1}s_1,e_{Y_2}s_2} = -\frac{1}{N_M} \sum_{\mathbf{k}'} V^{\eta e_{Y_1} e_{Y_2}}_{\mathbf{k}\mathbf{k}'} \langle \gamma_{-\mathbf{k}'e_{Y_2}\eta s_2} \gamma_{\mathbf{k}'e_{Y_1}-\eta s_1} \rangle. \tag{9}$$

Since the interaction $V$ function does not involve spin, we can decompose $\Delta^{\eta}_{\mathbf{k};e_{Y_1}s_1,e_{Y_2}s_2} = \sum_{S,M} \Delta^{\eta,SM}_{\mathbf{k};e_{Y_1}e_{Y_2}} \mathcal{S}^{SM}_{s_1s_2}$, where $S = 0$ for the spin singlet and $S = 1$ ($M = -S, \ldots, S$) for the spin triplet (SM Sec. VI G 1 [56]).

The gap function can be classified according to the discrete symmetries. The $C_{6v}$ group includes four 1D irreducible representations (irreps), e.g., $A_{1,2}$ and $B_{1,2}$, and two 2D irreps, $E_{1,2}$. The 1D irreps $A_{1,2}$ and $B_{1,2}$ channels differ by their $\hat{C}_{2z}$ eigenvalues, $\lambda_{C_{2z}} = +1$ for $A_{1,2}$ and $\lambda_{C_{2z}} = -1$ for $B_{1,2}$. Combining $\hat{C}_{2z}$ and reshuffling symmetries leads to $\Delta^{\eta}_{\mathbf{k};e_{Y_1},e_{Y_2}} = \lambda_{C_{2z}} \Delta^{\eta}_{\mathbf{k};e_{Y_2},e_{Y_1}}$ for the spin singlet and $\Delta^{\eta}_{\mathbf{k};e_{Y_1},e_{Y_2}} = -\lambda_{C_{2z}} \Delta^{\eta}_{\mathbf{k};e_{Y_2},e_{Y_1}}$ for the spin triplet. Thus, for intra-Chern-band pairing ($e_{Y_1} = e_{Y_2}$), the $A_{1,2}$ channel must be a spin singlet while the $B_{1,2}$ channel must be a spin triplet. Furthermore, the rotation $\hat{C}_{3z}$ ensures the existence of nodes at $\mathbf{K}_M$ for the gap function of any 1D irrep intra-Chern-band channel ($\Delta^{\eta}_{\mathbf{K}_M;e_Y,e_Y} = 0$), while the inter-Chern-band channel does not have such a constraint. The 2D irreps $E_1$ and $E_2$ have different $\hat{C}_{2z}$ eigenvalues, $\lambda_{C_{2z}} = +1$ for $E_2$ and $\lambda_{C_{2z}} = -1$ for $E_1$, similarly to the 1D irrep case. Consequently, the $E_2$ channel must be a spin singlet while the $E_1$ channel must be a spin triplet for intra-Chern-band pairings. $\hat{C}_{3z}$ guarantees nodes at $\Gamma_M$ for both intra- and inter-Chern-band channels, and it requires additional nodes at $\mathbf{K}_M$ for the inter-Chern-band channels for both 2D $E_{1,2}$ pairings. Besides discrete symmetries, the continuous $U(2)_{e_Y=1} \times U(2)_{e_Y=-1}$ spin symmetry in the chiral limit guarantees the singlet and triplet pairings of the inter-Chern-band channel to be degenerate in the chiral flat-band limit. The full symmetry analysis of the gap functions can be found in SM Sec. VI G [56] (see also Refs. [71,72] therein).

## IV. GAP EQUATIONS AND SELF-CONSISTENT SOLUTION OF PAIRING CHANNELS

The linearized gap equation (LGE) for the attractive interaction (7) can be derived by evaluating $\langle \gamma_{-\mathbf{k}'e_{Y_2}\eta s_2} \gamma_{\mathbf{k}'e_{Y_1}-\eta s_1} \rangle$ in Eq. (9) and expanding it to linear order of the gap function. In the chiral flat-band limit, e.g., the bandwidth is much smaller than the critical temperature $T_c$, the LGE is derived as

$$2k_B T \Delta^{\eta,SM}_{\mathbf{k};e_{Y_1}e_{Y_2}} = \frac{1}{N_M} \sum_{\mathbf{k}'} V^{\eta e_{Y_1} e_{Y_2}}_{\mathbf{k},\mathbf{k}'} \Delta^{-\eta,SM}_{\mathbf{k}';e_{Y_1}e_{Y_2}}. \tag{10}$$

This is an eigenequation problem for the matrix $V^{\eta e_{Y_1} e_{Y_2}}_{\mathbf{k},\mathbf{k}'}$: The $T_c$ is determined by the largest eigenvalue and the symmetry of the gap function is determined by that of its eigenvector. As mentioned, the only two independent components of the $V$ function (complex $V^{+++}_{\mathbf{k},\mathbf{k}'}$ and real $V^{++-}_{\mathbf{k},\mathbf{k}'}$) lead to two independent LGEs for the intra- and inter-Chern-band channels, respectively. The form of the LGE suggests that all the gap functions are doubly degenerate at $T_c$ in the flat-band limit. They belong either to two degenerate 1D irreps or one 2D irrep. We first numerically solve these two LGEs from Eq. (10), and find the forms of the gap functions with the largest eigenvalues, as shown in Fig. 1. Our numerical calculations show $k_B T_c \sim 0.21$ meV for the inter-Chern-band channel, slightly larger than $k_B T_c \sim 0.16$ meV for the intra-Chern-band channel. For the inter-Chern-band channels, the gap function is almost a constant in Fig. 1(a), featuring a fully gapped $s$-wave pairing with even $\hat{C}_{2z}$ parity ($A_1$ or $A_2$ irrep). In

the chiral flat-band limit, spin singlet and triplet pairings are degenerate, as required by the continuous $U(2) \times U(2)$ spin symmetry (SM Sec. VI E [56]). Including kinetic energy splits this degeneracy and makes the spin singlet $A_1$ irrep channel to have the highest $T_c$. For the intra-Chern-band channel, one can see nodes appearing at the $\Gamma_M$ in Fig. 1(b). As our previous symmetry analysis shows that the gap function should have nodes at $\mathbf{K}_M$ for the 1D irrep $(A_{1,2}, B_{1,2})$ and $\Gamma_M$ for the 2D irrep $(E_{1,2})$, numerical results should correspond to a 2D irrep. Numerically analyzing the symmetry property of the gap function suggests that the intra-Chern-band channel belongs to the 2D $E_2$ irrep with a spin singlet. Full numerical results are discussed in SM Secs. VI H 2 and VI H 3 [56].

Our results for the intra-Chern-band channels reveal a $d$-wave character of the gap. Using the heavy-fermion formalism of TBG [47], we analytically obtain $V^{\eta,e_Y,e_Y}_{\mathbf{k},\mathbf{k}'}$,

$$V^{\eta,e_Y,e_Y}_{\mathbf{k},\mathbf{k}'} = U^*_{e_Y,\mathbf{k}} U_{e_Y,\mathbf{k}'}, \quad U_{e_Y,\mathbf{k}} = \frac{\sqrt{V_0}}{k^2+b^2} k^2_{e_Y}, \tag{11}$$

with $k_{e_Y} = k_x + ie_Y k_y$ $(e_Y = \pm)$. This interaction allows us to solve the LGE analytically to obtain the $T_c$,

$$k_B T_c = \frac{\tilde{V}_0}{2}, \quad \tilde{V}_0 = \frac{1}{N_M}\sum_{\mathbf{k}} V_0 \frac{k^4}{(k^2+b^2)^2}, \tag{12}$$

where $V_0$ and $b$ are material-dependent parameters. The corresponding self-consistent gap function takes the $d$-wave form

$$\begin{pmatrix} \Delta^{+,00}_{\mathbf{k},e_Y e_Y} \\ \Delta^{-,00}_{\mathbf{k},e_Y e_Y} \end{pmatrix} = \Delta_{e_Y} \frac{k^2_{-e_Y}}{k^2+b^2} \begin{pmatrix} 1 \\ 1 \end{pmatrix}, \tag{13}$$

with $e_Y = \pm$ and $\Delta_{e_Y}$ a parameter to be determined. Time reversal, if it exists, requires $(\Delta^{-,00}_{\mathbf{k};--}, \Delta^{+,00}_{\mathbf{k};--}) = (\Delta^{+,00}_{\mathbf{k};++}, \Delta^{-,00}_{\mathbf{k};++})^*$. The $d$-wave nature of the gap function suggests the possibility of the nodal superconductivity. However, one should note that the single-particle Hamiltonian is *not* diagonal in the Chern-band basis. The Bogoliubov–de Gennes (BdG) spectrum must be checked with kinetic energy added. The BdG Hamiltonian for the intra-Chern-band pairing is block diagonal and one block $\mathcal{H}^{+,+}_{\mathrm{BdG}}$ on the basis $(\gamma^\dagger_{\mathbf{k},e_Y=\pm,+,s=\uparrow}, \gamma_{-\mathbf{k},e_Y=\pm,-,s=\downarrow})$ reads

$$H^{+,+}_{\mathrm{BdG}}(\mathbf{k}) = \begin{pmatrix} h_+(\mathbf{k}) & \Delta^+_{\mathbf{k}} \\ (\Delta^+_{\mathbf{k}})^\dagger & -h^\star_-(-\mathbf{k}) \end{pmatrix}, \tag{14}$$

with $h_\eta(\mathbf{k}) = (d_{0,\eta}(\mathbf{k}) - \mu)\zeta^0 + d_{x,\eta}(\mathbf{k})\zeta^x$ and $\Delta^+_{\mathbf{k}} = \mathrm{Diag}[\Delta^{+,00}_{\mathbf{k},++}, \Delta^{+,00}_{\mathbf{k},--}]$. Here, $d_{0,\eta}(\mathbf{k}) = [\epsilon_{+,\eta}(\mathbf{k}) + \epsilon_{-,\eta}(\mathbf{k})]/2$ and $d_{x,\eta}(\mathbf{k}) = [\epsilon_{+,\eta}(\mathbf{k}) - \epsilon_{-,\eta}(\mathbf{k})]/2$, where $\epsilon_{\pm,\eta}(\mathbf{k})$ are the eigenenergies for the two low-energy flat bands (per valley per spin) of the BM model $\hat{H}_{\mathrm{el}}$ (2). The corresponding energy spectrum can possess nodes when the pairing amplitudes of two Chern-band channels are equal, $|\Delta_{e_Y=+}| = |\Delta_{e_Y=-}| = \Delta_0$, which corresponds to the Euler pairing discussed in Refs. [32,73]. Point nodes appear at the location defined by two conditions, (1) $\cos[(\Phi_{\mathbf{k},-} - \Phi_{\mathbf{k},+})/2] = 0$, where $\Phi_{\mathbf{k},e_Y} = \varphi_{e_Y} - 2e_Y\theta_{\mathbf{k}}$ with $\Delta_{e_Y} = \Delta_0 e^{i\varphi_{e_Y}}$ and $k_{e_Y} = ke^{ie_Y\theta_{\mathbf{k}}}$, and (2) $d^2_{x,\mathbf{k}} = (d_{0,\mathbf{k}} - \mu)^2 + \Delta^2_{0,\mathbf{k}}$ with $\Delta_{0,\mathbf{k}} = \Delta_0 \frac{k^2}{k^2+b^2}$, as discussed in SM Sec. VI H 5 [56]. The first condition determines the momentum angle for the nodes while the second gives the momentum amplitude, thus together fixing

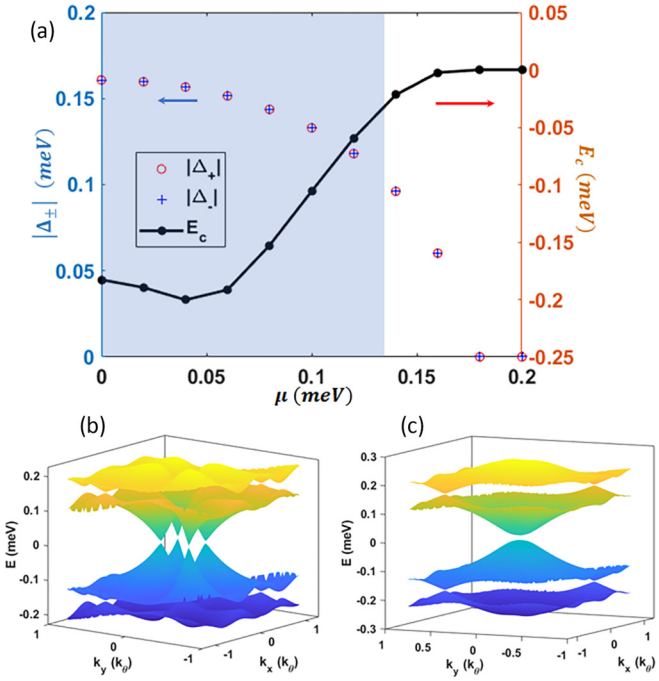


FIG. 2. (a) The superconductor order parameter amplitudes $|\Delta_\pm|$ (red circles and blue crosses) and the ground state energy (black dots) as a function of $\mu$. The superconducting phase has nodes in the shadowed regime. (b) and (c) show the BdG spectrum with and without nodes at $\mu = 0.04$ and 0.14 meV, respectively. The single-particle bandwidth is set around 0.3 meV.

the location of point nodes in the 2D momentum space. We next solve the self-consistent gap equation at zero temperature for the interaction form (11). With the gap function ansatz $\Delta_{\mathbf{k};e_Y} = \Delta_{e_Y} \frac{k^2_{-e_Y}}{k^2+b^2}$, we find a self-consistent gap equation

$$\Delta_{e_Y} = \frac{V_0}{N_M} \sum_{\mathbf{k}',e_{Y_1}} \frac{k'^2_{e_Y}}{k'^2+b^2} u_{-\mathbf{k}',e_Y e_{Y_1}} w^*_{-\mathbf{k}',e_Y e_{Y_1}}, \tag{15}$$

where $\psi_{\mathbf{k},e_{Y_1}} = (u_{\mathbf{k},\pm,e_{Y_1}}, w_{\mathbf{k},\pm e_{Y_1}})$ $(e_{Y_1} = \pm)$ are the eigenwave functions with the positive eigenenergies of the BdG Hamiltonian $H^{+,+}_{\mathrm{BdG}}(\mathbf{k})$ (14). Figure 2(a) shows the chemical potential dependence of the gap functions and the condensation energy. The Euler pairing $|\Delta_+| = |\Delta_-|$ is always energetically favored for a non-flat-bandwidth $\sim$0.3 meV, quite different from chiral $d$-wave pairing in doped graphene [26,74,75]. For the chemical potential $\mu$ below 0.1 meV, a nodal superconductor phase with four point nodes [Fig. 2(b)] located at the positions determined by two conditions discussed above [32]. With increasing $\mu$, four nodes move towards $\Gamma_M$ and eventually a gapped superconductor phase [Fig. 2(c)] appears for $\mu > 0.1$ meV.

The energy scale of the Coulomb interaction in TBG is $\sim$24 meV [58], much larger than the estimated energy scale of e-K-ph mediated attractive interaction $\sim$0.3 meV [76]. Near the Van Hove singularities of flat bands, the screening can significantly reduce the Coulomb interaction to a similar order as the e-K-ph mediated interaction due to the large DOS (SM Sec. VI H 7 [56]), thus making superconductivity from this mechanism possible. If, however, the DOS is that of

the Hartree-Fock bands of correlated insulators, the screening might not be enough to reduce the Coulomb interaction. Hence, superconductivity from this $K$-phonon flat bare band mechanism could appear only when the correlated insulator states are suppressed and the Coulomb interaction is strongly screened [77], which is consistent with the TBG experiments with different Coulomb screenings [78].

## V. CONCLUSION

In conclusion, we develop a theory for the projected e-K-ph interaction of the flat bands and the resulting superconductor pairing channels in TBG. We find the inter-Chern-band $s$-wave singlet pairing and the intra-Chern-band $d$-wave nematic singlet pairing have the highest $T_c$, and the $T_c$ of the inter-Chern-band channel is slightly higher than the intra-Chen-band channel. The intra-Chen-band channel can have nodes in a large parameter regime. From the estimate of the screened Coulomb interaction, we argue that this mechanism requires the correlated insulators to be suppressed.

## ACKNOWLEDGMENTS

We would like to acknowledge Biao Lian, Xi Dai, and Zhida Song for helpful discussion. B.A.B.'s heavy fermion in twisted bilayer research was supported by DOE Grant No. DE-SC0016239. B.A.B.'s sabbatical support also comes from the Simons Investigator Grant No. 404513, the Gordon and Betty Moore Foundation through Grant No. GBMF8685 towards the Princeton theory program, the Gordon and Betty Moore Foundation's EPiQS Initiative (Grant No. GBMF11070), Office of Naval Research (ONR Grant No. N00014-20-1-2303), and the European Research Council (ERC) under the European Union's Horizon 2020 research and innovation program (Grant Agreement No. 101020833). C.-X.L. also acknowledges the support through the Penn State MRSEC: Center for Nanoscale Science via NSF Award No. DMR-2011839 and NSF Grant No. PHY-1748958 to the Kavli Institute for Theoretical Physics (KITP). A.Y. acknowledges support from the Gordon and Betty Moore Foundation's EPiQS initiative Grant No. GBMF9469, DOE-BES Grant No. DE-FG02-07ER46419, Grant No. NSF-DMR-1904442, ARO MURI (W911NF-21-2-0147), and ONR Grant No. N00012-21-1-2592. C.-X.L. and A.Y. also acknowledge the support from the NSF-MERSEC (Grant No. MER- SEC DMR 2011750). Y.L.C. acknowledges the support from the Oxford-ShanghaiTech collaboration project and the Shanghai Municipal Science and Technology Major Project (Grant No. 2018SHZDZX02).

[1] Y. Cao, V. Fatemi, A. Demir, S. Fang, S. L. Tomarken, J. Y. Luo, J. D. Sanchez-Yamagishi, K. Watanabe, T. Taniguchi, E. Kaxiras *et al.*, Correlated insulator behaviour at half-filling in magic-angle graphene superlattices, Nature (London) **556**, 80 (2018).

[2] Y. Cao, V. Fatemi, S. Fang, K. Watanabe, T. Taniguchi, E. Kaxiras, and P. Jarillo-Herrero, Unconventional superconductivity in magic-angle graphene superlattices, Nature (London) **556**, 43 (2018).

[3] X. Lu, P. Stepanov, W. Yang, M. Xie, M. A. Aamir, I. Das, C. Urgell, K. Watanabe, T. Taniguchi, G. Zhang *et al.*, Superconductors, orbital magnets and correlated states in magic-angle bilayer graphene, Nature (London) **574**, 653 (2019).

[4] E. Codecido, Q. Wang, R. Koester, S. Che, H. Tian, R. Lv, S. Tran, K. Watanabe, T. Taniguchi, F. Zhang *et al.*, Correlated insulating and superconducting states in twisted bilayer graphene below the magic angle, Sci. Adv. **5**, eaaw9770 (2019).

[5] M. Yankowitz, S. Chen, H. Polshyn, Y. Zhang, K. Watanabe, T. Taniguchi, D. Graf, A. F. Young, and C. R. Dean, Tuning superconductivity in twisted bilayer graphene, Science **363**, 1059 (2019).

[6] Y. Cao, D. Rodan-Legrain, J. M. Park, N. F. Yuan, K. Watanabe, T. Taniguchi, R. M. Fernandes, L. Fu, and P. Jarillo-Herrero, Nematicity and competing orders in superconducting magic-angle graphene, Science **372**, 264 (2021).

[7] M. Oh, K. P. Nuckolls, D. Wong, R. L. Lee, X. Liu, K. Watanabe, T. Taniguchi, and A. Yazdani, Evidence for unconventional superconductivity in twisted bilayer graphene, Nature (London) **600**, 240 (2021).

[8] X. Liu, Z. Wang, K. Watanabe, T. Taniguchi, O. Vafek, and J. Li, Tuning electron correlation in magic-angle twisted bilayer graphene using Coulomb screening, Science **371**, 1261 (2021).

[9] Y. Saito, J. Ge, K. Watanabe, T. Taniguchi, and A. F. Young, Independent superconductors and correlated insulators in twisted bilayer graphene, Nat. Phys. **16**, 926 (2020).

[10] H. S. Arora, R. Polski, Y. Zhang, A. Thomson, Y. Choi, H. Kim, Z. Lin, I. Z. Wilson, X. Xu, J.-H. Chu *et al.*, Superconductivity in metallic twisted bilayer graphene stabilized by $WSe_2$, Nature (London) **583**, 379 (2020).

[11] E. Y. Andrei and A. H. MacDonald, Graphene bilayers with a twist, Nat. Mater. **19**, 1265 (2020).

[12] J. Liu and X. Dai, Orbital magnetic states in moiré graphene systems, Nat. Rev. Phys. **3**, 367 (2021).

[13] Y. H. Kwan, G. Wagner, T. Soejima, M. P. Zaletel, S. H. Simon, S. A. Parameswaran, and N. Bultinck, Kekulé spiral order at all nonzero integer fillings in twisted bilayer graphene, Phys. Rev. X **11**, 041063 (2021).

[14] K. P. Nuckolls, R. L. Lee, M. Oh, D. Wong, T. Soejima, J. P. Hong, D. Călugăru, J. Herzog-Arbeitman, B. A. Bernevig, K. Watanabe *et al.*, Quantum textures of the many-body wavefunctions in magic-angle graphene, Nature (London) **620**, 525 (2023).

[15] D. Călugăru, N. Regnault, M. Oh, K. P. Nuckolls, D. Wong, R. L. Lee, A. Yazdani, O. Vafek, and B. A. Bernevig, Spectroscopy of twisted bilayer graphene correlated insulators, Phys. Rev. Lett. **129**, 117602 (2022).

[16] J. Kang, B. A. Bernevig, and O. Vafek, Cascades between light and heavy fermions in the normal state of magic-angle twisted bilayer graphene, Phys. Rev. Lett. **127**, 266402 (2021).

[17] J. Kang and O. Vafek, Symmetry, maximally localized Wannier states, and a low-energy model for twisted bilayer graphene narrow bands, Phys. Rev. X **8**, 031088 (2018).

[18] J. Kang and O. Vafek, Strong coupling phases of partially filled twisted bilayer graphene narrow bands, Phys. Rev. Lett. **122**, 246401 (2019).

[19] O. Vafek and J. Kang, Renormalization group study of hidden symmetry in twisted bilayer graphene with Coulomb interactions, Phys. Rev. Lett. **125**, 257602 (2020).

[20] E. Khalaf, S. Chatterjee, N. Bultinck, M. P. Zaletel, and A. Vishwanath, Charged skyrmions and topological origin of superconductivity in magic-angle graphene, Sci. Adv. **7**, eabf5299 (2021).

[21] E. Khalaf, P. Ledwith, and A. Vishwanath, Symmetry constraints on superconductivity in twisted bilayer graphene: Fractional vortices, 4*e* condensates, or nonunitary pairing, Phys. Rev. B **105**, 224508 (2022).

[22] H. C. Po, L. Zou, A. Vishwanath, and T. Senthil, Origin of Mott insulating behavior and superconductivity in twisted bilayer graphene, Phys. Rev. X **8**, 031089 (2018).

[23] Y.-Z. You and A. Vishwanath, Superconductivity from valley fluctuations and approximate SO(4) symmetry in a weak coupling theory of twisted bilayer graphene, npj Quantum Mater. **4**, 16 (2019).

[24] B. Lian, Z. Wang, and B. A. Bernevig, Twisted bilayer graphene: A phonon-driven superconductor, Phys. Rev. Lett. **122**, 257002 (2019).

[25] F. Wu, A. H. MacDonald, and I. Martin, Theory of phonon-mediated superconductivity in twisted bilayer graphene, Phys. Rev. Lett. **121**, 257001 (2018).

[26] F. Wu, Topological chiral superconductivity with spontaneous vortices and supercurrent in twisted bilayer graphene, Phys. Rev. B **99**, 195114 (2019).

[27] F. Wu, E. Hwang, and S. Das Sarma, Phonon-induced giant linear-in-$T$ resistivity in magic angle twisted bilayer graphene: Ordinary strangeness and exotic superconductivity, Phys. Rev. B **99**, 165112 (2019).

[28] F. Wu and S. Das Sarma, Identification of superconducting pairing symmetry in twisted bilayer graphene using in-plane magnetic field and strain, Phys. Rev. B **99**, 220507(R) (2019).

[29] D. V. Chichinadze, L. Classen, and A. V. Chubukov, Nematic superconductivity in twisted bilayer graphene, Phys. Rev. B **101**, 224513 (2020).

[30] R. M. Fernandes and L. Fu, Charge-4*e* superconductivity from multicomponent nematic pairing: Application to twisted bilayer graphene, Phys. Rev. Lett. **127**, 047001 (2021).

[31] Y. Wang, J. Kang, and R. M. Fernandes, Topological and nematic superconductivity mediated by ferro-SU(4) fluctuations in twisted bilayer graphene, Phys. Rev. B **103**, 024506 (2021).

[32] J. Yu, M. Xie, F. Wu, and S. Das Sarma, Euler-obstructed nematic nodal superconductivity in twisted bilayer graphene, Phys. Rev. B **107**, L201106 (2023).

[33] G. Sharma, M. Trushin, O. P. Sushkov, G. Vignale, and S. Adam, Superconductivity from collective excitations in magic-angle twisted bilayer graphene, Phys. Rev. Res. **2**, 022040(R) (2020).

[34] H. Isobe, N. F. Q. Yuan, and L. Fu, Unconventional superconductivity and density waves in twisted bilayer graphene, Phys. Rev. X **8**, 041041 (2018).

[35] B. Roy and V. Juričić, Unconventional superconductivity in nearly flat bands in twisted bilayer graphene, Phys. Rev. B **99**, 121407(R) (2019).

[36] T. J. Peltonen, R. Ojajärvi, and T. T. Heikkilä, Mean-field theory for superconductivity in twisted bilayer graphene, Phys. Rev. B **98**, 220504(R) (2018).

[37] D. M. Kennes, J. Lischner, and C. Karrasch, Strong correlations and $d + id$ superconductivity in twisted bilayer graphene, Phys. Rev. B **98**, 241407(R) (2018).

[38] J. Gonzalez and T. Stauber, Kohn-Luttinger superconductivity in twisted bilayer graphene, Phys. Rev. Lett. **122**, 026801 (2019).

[39] T. Cea and F. Guinea, Coulomb interaction, phonons, and superconductivity in twisted bilayer graphene, Proc. Natl. Acad. Sci. USA **118**, e2107874118 (2021).

[40] G. Shavit, E. Berg, A. Stern, and Y. Oreg, Theory of correlated insulators and superconductivity in twisted bilayer graphene, Phys. Rev. Lett. **127**, 247703 (2021).

[41] C.-C. Liu, L.-D. Zhang, W.-Q. Chen, and F. Yang, Chiral spin density wave and $d + id$ superconductivity in the magic-angle-twisted bilayer graphene, Phys. Rev. Lett. **121**, 217001 (2018).

[42] M. Fidrysiak, M. Zegrodnik, and J. Spałek, Unconventional topological superconductivity and phase diagram for an effective two-orbital model as applied to twisted bilayer graphene, Phys. Rev. B **98**, 085436 (2018).

[43] Y.-Z. Chou, Y.-P. Lin, S. Das Sarma, and R. M. Nandkishore, Superconductor versus insulator in twisted bilayer graphene, Phys. Rev. B **100**, 115128 (2019).

[44] V. Kozii, H. Isobe, J. W. F. Venderbos, and L. Fu, Nematic superconductivity stabilized by density wave fluctuations: Possible application to twisted bilayer graphene, Phys. Rev. B **99**, 144507 (2019).

[45] I. Maccari, J. Carlström, and E. Babaev, Prediction of time-reversal-symmetry breaking fermionic quadrupling condensate in twisted bilayer graphene, Phys. Rev. B **107**, 064501 (2023).

[46] C. Chen, K. P. Nuckolls, S. Ding, W. Miao, D. Wong, M. Oh, R. L. Lee, S. He, C. Peng, D. Pei *et al.*, Strong inter-valley electron-phonon coupling in magic-angle twisted bilayer graphene, arXiv:2303.14903.

[47] Z.-D. Song and B. A. Bernevig, Magic-angle twisted bilayer graphene as a topological heavy fermion problem, Phys. Rev. Lett. **129**, 047601 (2022).

[48] D. Călugăru, M. Borovkov, L. L. H. Lau, P. Coleman, Z.-D. Song, and B. A. Bernevig, Twisted bilayer graphene as topological heavy fermion: II. Analytical approximations of the model parameters, Low Temp. Phys. **49**, 640 (2023).

[49] H. Hu, G. Rai, L. Crippa, J. Herzog-Arbeitman, D. Călugăru, T. Wehling, G. Sangiovanni, R. Valentí, A. M. Tsvelik, and B. A. Bernevig, Symmetric Kondo lattice states in doped strained twisted bilayer graphene, Phys. Rev. Lett. **131**, 166501 (2023).

[50] H. Hu, B. A. Bernevig, and A. M. Tsvelik, Kondo lattice model of magic-angle twisted-bilayer graphene: Hund's rule, local-moment fluctuations, and low-energy effective theory, Phys. Rev. Lett. **131**, 026502 (2023).

[51] L. L. Lau and P. Coleman, Topological mixed valence model for twisted bilayer graphene, arXiv:2303.02670.

[52] A. Datta, M. J. Calderon, A. Camjayi, and E. Bascones, Heavy quasiparticles and cascades without symmetry breaking in twisted bilayer graphene, Nat. Commun. **14**, 5036 (2023).

[53] J. Yu, M. Xie, B. A. Bernevig, and S. Das Sarma, Magic-angle twisted symmetric trilayer graphene as a topological heavy-fermion problem, Phys. Rev. B **108**, 035129 (2023).

[54] Y.-Z. Chou and S. Das Sarma, Kondo lattice model in magic-angle twisted bilayer graphene, Phys. Rev. Lett. **131**, 026501 (2023).

[55] G.-D. Zhou, Y.-J. Wang, N. Tong, and Z.-D. Song, Kondo phase in twisted bilayer graphene, Phys. Rev. B **109**, 045419 (2024).

[56] See Supplemental Material at http://link.aps.org/supplemental/10.1103/PhysRevB.110.045133 for details of the derivations of electron-phonon interaction in graphene and its projection to the flat bands of twisted bilayer graphene, symmetry analysis of the phonon-mediated electron-electron interaction and irreducible superconductor pairing channels, the linearized and $T = 0$ gap equations, the superconductor ground state energy, and the Coulomb screening effect.

[57] R. Bistritzer and A. H. MacDonald, Moiré bands in twisted double-layer graphene, Proc. Natl. Acad. Sci. USA **108**, 12233 (2011).

[58] B. A. Bernevig, Z.-D. Song, N. Regnault, and B. Lian, Twisted bilayer graphene. III. Interacting Hamiltonian and exact symmetries, Phys. Rev. B **103**, 205413 (2021).

[59] Z.-D. Song, B. Lian, N. Regnault, and B. A. Bernevig, Twisted bilayer graphene. II. Stable symmetry anomaly, Phys. Rev. B **103**, 205412 (2021).

[60] H. C. Po, L. Zou, T. Senthil, and A. Vishwanath, Faithful tight-binding models and fragile topology of magic-angle bilayer graphene, Phys. Rev. B **99**, 195455 (2019).

[61] G. Tarnopolsky, A. J. Kruchkov, and A. Vishwanath, Origin of magic angles in twisted bilayer graphene, Phys. Rev. Lett. **122**, 106405 (2019).

[62] Z. Song, Z. Wang, W. Shi, G. Li, C. Fang, and B. A. Bernevig, All magic angles in twisted bilayer graphene are topological, Phys. Rev. Lett. **123**, 036401 (2019).

[63] J. Ahn, S. Park, and B.-J. Yang, Failure of Nielsen-Ninomiya theorem and fragile topology in two-dimensional systems with space-time inversion symmetry: Application to twisted bilayer graphene at magic angle, Phys. Rev. X **9**, 021013 (2019).

[64] A. H. Castro Neto, F. Guinea, N. M. R. Peres, K. S. Novoselov, and A. K. Geim, The electronic properties of graphene, Rev. Mod. Phys. **81**, 109 (2009).

[65] R. Sahoo and R. R. Mishra, Phonon dispersion of graphene revisited, J. Exp. Theor. Phys. **114**, 805 (2012).

[66] E. Thingstad, A. Kamra, J. W. Wells, and A. Sudbø, Phonon-mediated superconductivity in doped monolayer materials, Phys. Rev. B **101**, 214513 (2020).

[67] J. Maultzsch, S. Reich, C. Thomsen, H. Requardt, and P. Ordejón, Phonon dispersion in graphite, Phys. Rev. Lett. **92**, 075501 (2004).

[68] M. Mohr, J. Maultzsch, E. Dobardžić, S. Reich, I. Milošević, M. Damnjanović, A. Bosak, M. Krisch, and C. Thomsen, Phonon dispersion of graphite by inelastic x-ray scattering, Phys. Rev. B **76**, 035439 (2007).

[69] J. R. Schrieffer and P. A. Wolff, Relation between the Anderson and Kondo Hamiltonians, Phys. Rev. **149**, 491 (1966).

[70] N. Bultinck, E. Khalaf, S. Liu, S. Chatterjee, A. Vishwanath, and M. P. Zaletel, Ground state and hidden symmetry of magic-angle graphene at even integer filling, Phys. Rev. X **10**, 031034 (2020).

[71] L. Savary, J. Ruhman, J. W. F. Venderbos, L. Fu, and P. A. Lee, Superconductivity in three-dimensional spin-orbit coupled semimetals, Phys. Rev. B **96**, 214514 (2017).

[72] M. Sigrist and K. Ueda, Phenomenological theory of unconventional superconductivity, Rev. Mod. Phys. **63**, 239 (1991).

[73] J. Yu, Y.-A. Chen, and S. Das Sarma, Euler-obstructed Cooper pairing: Nodal superconductivity and hinge Majorana zero modes, Phys. Rev. B **105**, 104515 (2022).

[74] A. M. Black-Schaffer and C. Honerkamp, Chiral $d$-wave superconductivity in doped graphene, J. Phys.: Condens. Matter **26**, 423201 (2014).

[75] R. Nandkishore, L. S. Levitov, and A. V. Chubukov, Chiral superconductivity from repulsive interactions in doped graphene, Nat. Phys. **8**, 158 (2012).

[76] Note that our calculation is performed in the chiral limit, so we may underestimate the electron-phonon coupling strength.

[77] Y.-J. Wang, G.-D. Zhou, S.-Y. Peng, B. Lian, and Z.-D. Song, Molecular pairing in twisted bilayer graphene superconductivity, arXiv:2402.00869.

[78] P. Stepanov, I. Das, X. Lu, A. Fahimniya, K. Watanabe, T. Taniguchi, F. H. Koppens, J. Lischner, L. Levitov, and D. K. Efetov, Untying the insulating and superconducting orders in magic-angle graphene, Nature (London) **583**, 375 (2020).